Progress In Electromagnetics Research C, Vol. 50, 47–56, 2014

A Very Compact Novel Multi-Band BPF for Recent Mobile/Satellite Communication Systems

Hesham A. Mohamed[1, *], Heba B. El-Shaarawy[2], Esmat A. Abdallah[1], and Hadia M. El-Hennawy[3]

Abstract—This paper presents a novel compact dual-tri bandpass microstrip filter employing meander and open stub loaded resonators. With the proposed technique, a simple transformation from dual-band to tri-band BPF is realized. A novel structure using embedded resonators is designed to generate multi-band response. The main resonators control the low-band resonant frequency, the meander resonators control the two high-band resonant frequency and the open stub resonators control the high-band resonant frequency. The meander/stub resonators are embedded into the main spiral resonators, which makes the filter compact where its size is reduced by 64% compared to traditional filters. Passbands improvements and high selectivity are realized by the short circuit stubs which generate additional transmission zeros. The proposed filter has advantages such as low insertion loss, compact size and high selectivity. The theory is validated using the commercial full-wave solver CST 2012. Finally, the proposed structure is implemented and the measurement results are found to be in good agreement with the simulation results.

1. INTRODUCTION

In modern wireless and mobile/satellite communication systems, the increasing demand for wireless communication applications necessitates RF transceivers operating in multiple separated frequency bands. For example, long term evolution systems for mobile communications (LTE) operate at L_1 band 0.75 GHz, 1.21 GHz for L_2 band of global positioning band (GPS), and 2.1 GHz for UMTS. Therefore, the multiband filters have been gaining wide attention in recent years. Dual-band filter is the most common multiband filter, which has been analyzed deeply in many articles with various configurations [1–6]. The dual-band filters were reported in [4–6] using SLR. Tri-band microstrip planar filters were also reported in [7–13]. However, RF filter is a basic and important component in the modern wireless communication system, and bandpass filter with the features of micro-package, good performance, low cost and ease of use has been the focus of device miniaturization. With the development of wireless communications, spectrum has become increasingly crowded, and the needs for multi-frequency filter applications are also gradually increasing. Special wireless transceiver is required to work in a number of respective bands, in order to allow users to adopt an individual terminal to achieve different services.

Therefore, designing a dual/tri-band filter at low cost and with high performance is currently of great interest. Microstrip multi-band filters can be easily mounted on a dielectric substrate and provide a more flexible design of the circuit layout [4]. The stub-loaded resonators filters have been known for years. The compact high performance microwave multi-band filters are highly desirable in wireless communication systems. The design of different multi-band filters was discussed by many authors [3–9], where they proposed multi-band filters, but the configurations still occupied a large circuit area and had

Received 13 March 2014, Accepted 16 April 2014, Scheduled 9 May 2014

* Corresponding author: Hesham Abd Elhady Mohamed (hesham_280@yahoo.com).

[1] Electronics Research Institute, Giza, Egypt. [2] Electronics and Communication Engineering Department, Faculty of Engineering, Cairo University, Giza, Egypt. [3] Electronics and Communication Engineering Department, Faculty of Engineering, Ain Shams University, Cairo, Egypt.

complex designs, which are not suitable for wireless communication systems where the miniaturization is an important factor. Therefore, it is desirable to develop new types of dual-band microstrip resonators not only for offering alternative designs, but also for miniaturizing filters. The filter is simulated by CST 2012 on the RT/Duroid 3010 with a dielectric constant of $\varepsilon_r = 10.2$, a thickness h of 0.635 mm and a loss tangent of 0.0025.

The organization of the paper is as follows. Section 2 presents the structure and design considerations of microstrip resonators. A theoretical solution is derived to show the dual-band BPF operation in Section 3. Section 4 gives the design of dual band microstrip BPF with good isolation. Section 5 introduces the design of a new tri-band filter using the dual-band BPF. The results and discussions are given in Section 6 with comparisons with other filters. Finally, conclusions are given in Section 7.

2. STRUCTURE AND DESIGN CONSIDERATIONS OF MICROSTRIP RESONATORS

The conventional topology of this type of microstrip bandpass filter is second order filter having an asymmetric structure. The filter consists of two open loop resonators in a C-shape configuration with half-wavelength as in Figure 1(a), which normally exhibits a single passband response at LTE band 750 MHz with size of $20 \times 40.2\,\text{mm}^2$ as in [1]. The main C-shape resonator structure has been replaced with spiral-shaped resonator embedded inside the compact size of open loop resonators, the new size is 24.2 mm × 12 mm ($0.15\lambda_g \times 0.075\lambda_g$) as in Figure 1(b), with 64% size reduction as compared to the same traditional size of 40.2 mm × 20 mm ($0.25\lambda_g \times 0.125\lambda_g$) at λ_g is the guide wavelength at LTE band, with the non-zero feed as shown in Figure 2(a). Spiral-shaped resonators can also be utilized to design single-passband filters in which the harmonic responses can be suppressed by utilizing several cascaded spiral with the same fundamental frequency, as shown in Figure 2(b). The passband response has two transmission zeros to generate a Chebyshev response. Figure 2(b) depicts compares the simulated results of two shapes. Some slight discrepancy is observed in passband centered at 0.75 GHz, the passband insertion loss approximately 0.34 dB in both shapes and the return loss are enhanced from −11 dB in C-shape to −30 dB in spiral shape. A bandpass response with wide stopband is observed in spiral shaped resonator. It can be seen that the 2nd order modes rejection levels are enhanced by 25 dB at the second harmonic frequencies when the spiral shaped resonator is employed. The fractional bandwidth is 11.2%. Meanwhile, operating lower transmission zero are 0.59 GHz and 0.603 GHz, whereas the upper transmission zero excitations 0.88 GHz and 0.96 GHz in C shape and spiral shape, respectively. Then the unloaded Q is defined as the inverse of the half-power fractional bandwidth of the resonator and measure of the losses in the filter. These unloaded Q is equal to 7.5 and 9 in C-shaped resonator and spiral-shaped resonators, respectively.

It has been shown that the proposed microstrip single-band filter has the disadvantages of low return loss, not good rejection of 2nd order modes, and the size is not compact and cannot be adjusted as shown in Figure 2(b). In this modified filter structure, which is not periodical, the 2nd harmonic at

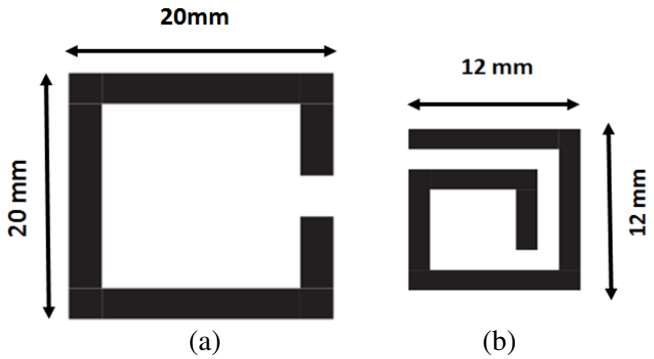

Figure 1. Conventional C-shaped open-loop resonator. (b) Proposed spiral-shaped resonator.

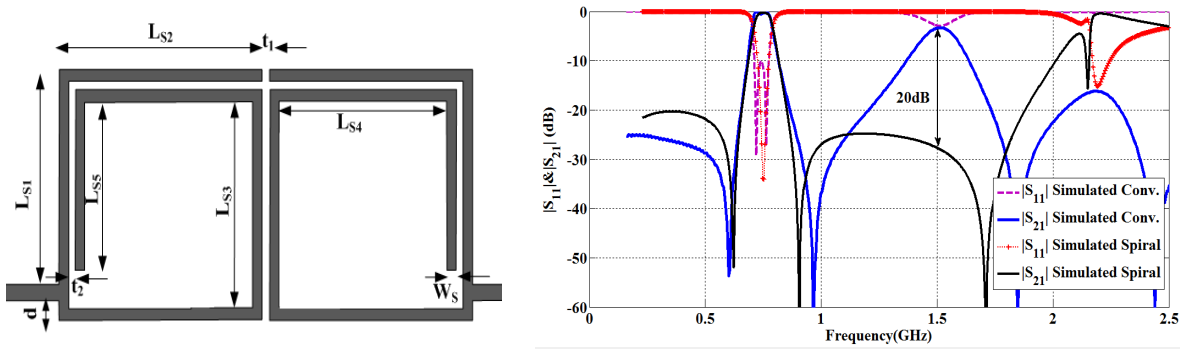

(a) (b)

Figure 2. (a) Structure of the proposed single-band BPF with spiral-shaped resonator. (b) *S*-parameters of the spiral-shaped resonator filter and conventional C-shaped BPF.

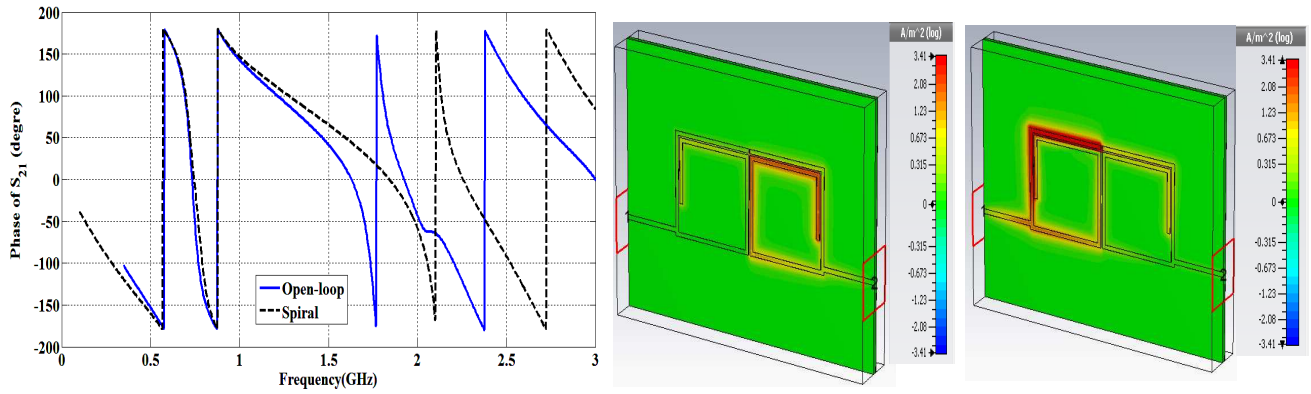

(a) (b) (c)

Figure 3. (a) Simulated phase response of S_{21} for resonators, 3D current distribution density at two transmission zeros at (b) 0.59 GHz, (c) 0.88 GHz.

1.5 GHz is eliminated, and all stopbands obtain the rejection levels about 20 dB as in Figure 2(b).

Figure 3(a) shows the phase response for S_{21} against frequencies. From shown results it can be obviously found that the fundamental resonating frequencies of their various resonators are simultaneously designed around 0.75 GHz, and the open-loop resonator and spiral-shaped resonator are identical. By the property of non-periodical resonating frequency for spiral-shaped resonator, it can be used effectively into designing the BPF applications. The operating mechanism of two transmission zeros can be explained by the current distributions. As shown in Figures 3(b) and (c), the surface current distributions at the resonant frequencies of 0.59 and 0.88 GHz simulated by CST 2012 are given, respectively. It can be observed that a large surface current density is induced on the end of the first spiral-shaped resonator when the proposed filter operating at the lower transmission zero (0.59 GHz), whereas for the upper transmission zero excitations (0.88 GHz), the current distributions become more concentrated along the end of embedded half-wavelength second spiral resonator.

3. DESIGN OF DUAL-BAND MICROSTRIP BANDPASS FILTER

In this section, a variable characteristic impedance transmission line that can be used in the design of dual-band BPF is presented. The proposed dual-band filter offers a fixed first passband and a tunable second passband. The tuning of the second passband is achieved by varying the characteristic impedance of open shunt stub line in a SLR [4]. Figure 4(a) shows the proposed structure of the tunable SLR, which consists of series resonators and an open shunt stub at the junction point between the series

resonators. Assume Y_1, θ_1, and Y_2, θ_2 as the characteristic admittance and electrical length of the series resonators and the open shunt stub, respectively. The input admittance of the proposed structure is given by:

$$Y_{in} = jY_1 \frac{2Y_1 \tan\theta_1 + Y_2 \tan\theta_2}{Y_1 - (Y_1 \tan\theta_1 + Y_2 \tan\theta_2)\tan\theta_1} \tag{1}$$

The resonant condition can be obtained by setting $Y_{in1} = 0$ which is obtained as:

$$2Y_1 \tan(a\theta_1) + Y_2 \tan(a\theta_2) = 0 \tag{2}$$

where (a) is the ratio of the higher mode resonant frequency (f_r) to the fundamental resonant frequency (f_1). The fundamental resonance can be obtained from (2) by setting $a = 1$ and $\theta_1 = 90$.

The relationship between the first two resonant frequency ratios (f_r/f_1) and impedance ratio $(K = Z_2/Z_1)$ of the SLR is plotted in Figure 4(b) using MATLAB code. From Figure 4(b), it is clear that by keeping the electrical length of the open shunt stub fixed, the frequency ratio (f_r/f_1) can be tuned by varying the impedance (Z_2/Z_1) of the SLR. This SLR characteristic is applied in the design of the dual-band BPF with the tunable second passband. These two resonances can be obtained by [4]:

$$f_1 = \frac{(2n-1)C}{2\pi L_1 \sqrt{\varepsilon_{eff}}}, \tag{3}$$

and

$$f_r = \frac{nC}{(L_1 + 2L_2)\sqrt{\varepsilon_{eff}}} \tag{4}$$

where C is the speed of light in free space, n the mode number $(n = 1, 3, 5, \ldots)$, L_1 the length of the spiral-shaped microstrip line, $L_2 = L_{M1}\,(9\,\text{mm}) + 3L_{M2}\,(3.2\,\text{mm}) + 3L_{M3}\,(6\,\text{mm})$ the meander length as in Figure 5(a), and ε_{eff} the effective dielectric constant of the substrate. It can be observed that the fundamental odd-mode resonant frequency is not affected by the open-circuited stub [4]. For example, the L_1 band of LTE of mobile communications and L_2 band of global positioning systems (GPS) for satellite applications operate at both 0.75 GHz and 1.221 GHz. The dual-passband operation for RF circuits has become a demand after the recent development in the wireless communication. The center frequencies of the two passbands are 0.75 GHz and 1.21 GHz. The corresponding resonant frequency ratio is calculated as $a = f_r/f_1 = 1.21/0.75 = 1.62$, Figure 4(b). The relationship between impedance ratio K and normalized spurious resonant frequency f_r/f_0 then chosen to be $Z_1 = 53\,\Omega$, $Z_2 = 40\,\Omega$ at $K = 0.78$. Figure 5(b) shows the comparison of S-parameter simulation and measurement results of the proposed filter. It is found that the measurement and simulation results are matched. The measured results of the planar dual-band bandpass filter based on a novel feed scheme have a central frequency of 0.75 GHz and 1.21 GHz for LTE and GPS applications. The first passband with center frequency of 0.75 GHz has an insertion loss less than 0.95 dB and return loss greater than 17 dB. The second

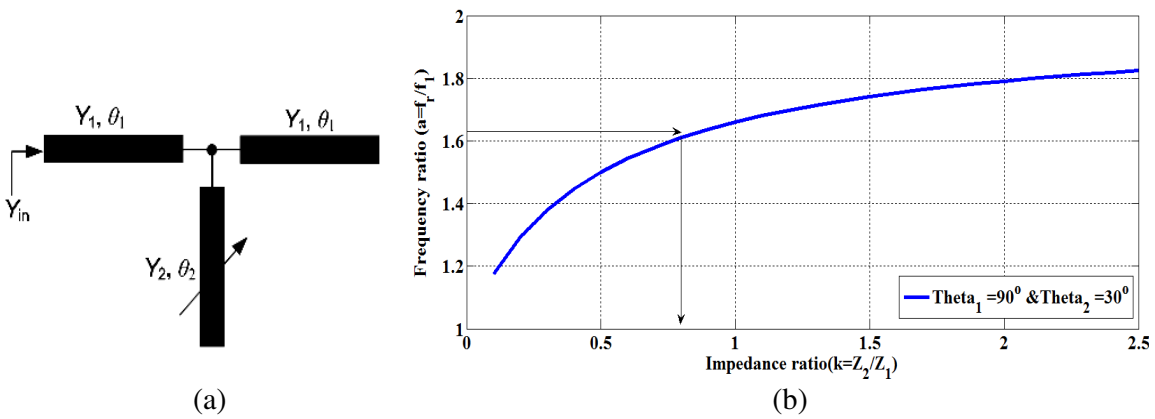

(a) (b)

Figure 4. (a) Structure of tunable stub loaded resonator. (b) Dependence of resonant frequency ratio according to characteristic impedance of open stub.

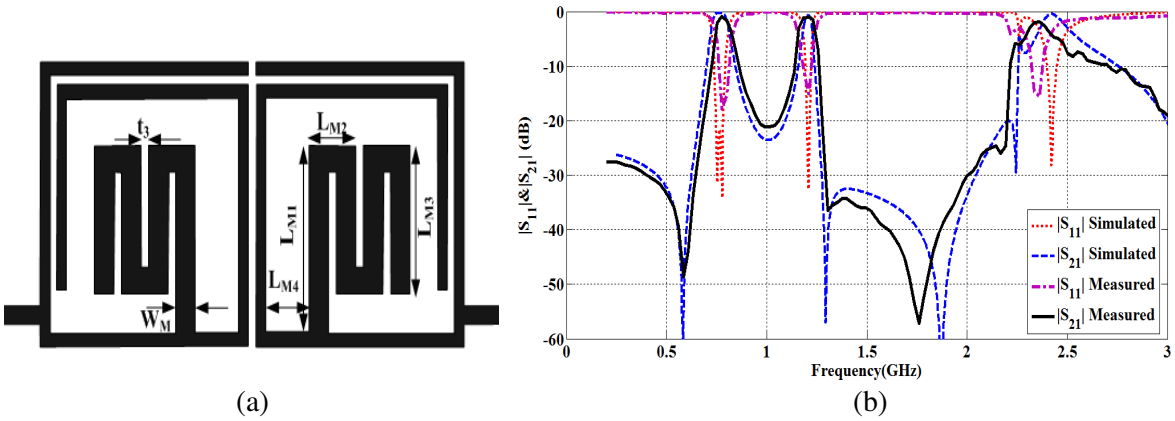

Figure 5. (a) Dual-band bandpass filter (DB-BPF) structure with spiral shape resonator, and meander open stub resonators. (b) Frequency response of dual-band BPF.

passband with center frequency of 1.214 GHz has insertion loss less than 0.8 dB and return loss greater than 14 dB.

4. DESIGN OF DUAL-BAND MICROSTRIP BANDPASS FILTERS WITH GOOD IN-BETWEEN ISOLATION

Improving the isolation between the first and second bandpasses of the filter is investigated. Figure 6(a) shows the schematic diagram. Short-circuited resonators are added to the first filter. In this configuration, the filter has a quasi-elliptic-function response with the symmetric feeding lines. With the asymmetric feeding lines, the filter achieves a Chebyshev response [3]. This is different from that of the first filter. Furthermore, the two output signals are identical. Hence, only one 180° 50-ohm delay line is used for signal cancellation, which saves circuit size. The second bandpass filter shows better stopband responses. The importance of keeping filter structures to a minimum size and weight, low insertion loss, high frequency selectivity has been widely recognized in the current filter.

This symmetric feed structure is referred to as a non-0 feed structure in Figure 6(a). There is no transmission zero, which implies $S_{21} \neq 0$, while another feed structure is 0° feed structure which has a 0 difference between the electric delays of the lower and upper paths. 0° feed structures [14] are realized at both the lower and upper bands to generate additional transmission zeros. The proposed filter shows advantages such as low insertion loss, compact size and low selectivity between pass bands. 0° feed

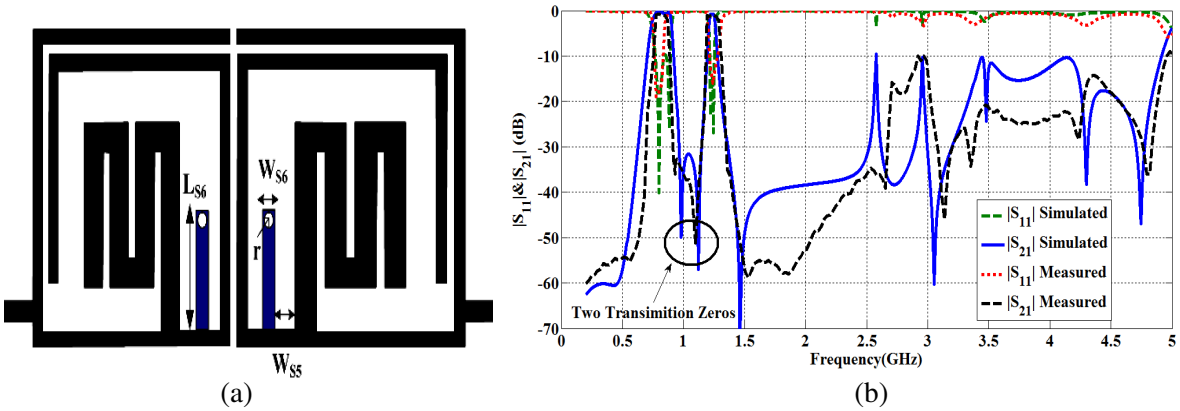

Figure 6. (a) Configuration of the proposed DB = BPF with short stub lines. (b) Frequency response of DB-BPF with short stubs.

structure which has a pair of transmission zeros in the stopbands is realized to improve the selectivity of the filter. At the frequencies where transmission zeros exist, $S_{21} = 0$. So, we establish the short circuit stub in the structure of the two symmetric resonators.

Figure 6(a) shows the transformation process to design an embedded-scheme resonator for DB-BPF. In Figure 6(a) a quad-wavelength short stub loaded SLR is shown and has the same size of the filter. Due to the existence of via hole, magnetic coupling takes up dominant position on the short stub loaded SLR. So, transmission zeros near the two pass bands can be generated by short stub loaded with via holes, due to the counteraction between electric and magnetic fields. These transmission zeros permit to improve selectivity and suppression of higher order modes. The dimensions of the short circuit stubs are: $L_{s5} = 3.35\,\text{mm}$, $W_{s5} = 0.8\,\text{mm}$, $W_{s6} = 0.5\,\text{mm}$ and $r = 0.25\,\text{mm}$.

The operating mechanism of dual-band filter with two transmission zeros can be explained by the current distributions. To validate the characteristics, the proposed dual-band filter is fabricated and measured. Figure 6(b) depicts the simulated and measured results of the proposed filter simultaneously. The simulated/measured minimum insertion losses are 0.79 dB/1.3 dB at 0.75 GHz band and 0.88 dB/0.96 dB at 1.21 GHz band, and the simulated/measured minimum return loss is 20 dB/15 dB at 0.75 GHz band and 28.2 dB/24.3 dB at 1.21 GHz band.

The measured 3 dB bandwidths are 11% and 7.8%. Two pairs of transmission zeros outside the passbands are located at 0.67 GHz, 0.97 GHz, 1.12 GHz and 1.48 GHz, which improve the out-of-band suppression and selectivity. In addition, the filter exhibits a wide stopband up to 5 GHz due to stepped impedance resonators and proposes the first spurious resonant frequency of the dispersion effect. As shown in Figures 7(a) and (b), the surface current distributions at the resonance frequencies of 0.97 and 1.121 GHz simulated by CST are given, respectively. It can be observed that a large surface current density is induced on short stub loaded SLR when the proposed filter operates at the lower band (0.75 GHz), whereas for the upper-band excitations (1.21 GHz), the current distributions become more concentrated along the embedded spiral-shaped resonators. Figure 7(c) shows a photograph of the fabricated dual-band filter.

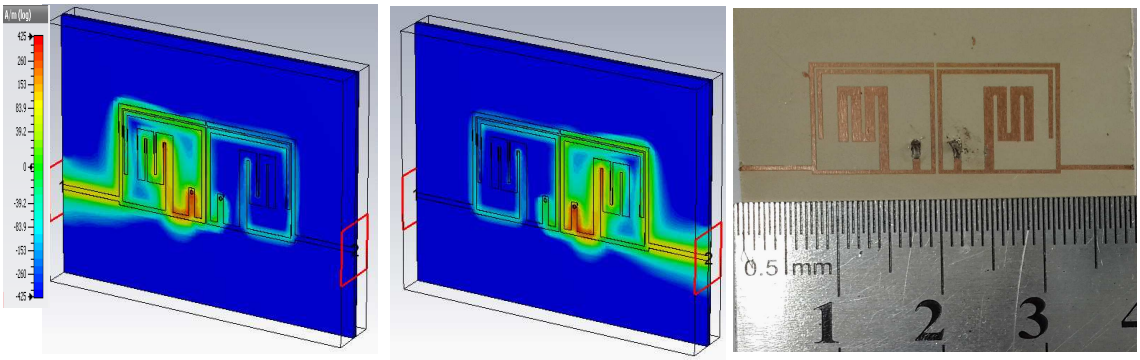

(a) (b) (c)

Figure 7. Surface current distributions at two transmission zero of the proposed filter, (a) 0.67 GHz, (b) 1.12 GHz, (c) photograph of the fabricated dual-band filter.

5. DESIGN OF A NEW TRI-BAND USING THE DUAL-BAND BP

The urgent need for dual- and multi-band microwave filters, with compact, high-performance RF front-end, capable of operating at more than one frequency band, plays an important role in a variety of modern wireless systems, such as LTE, GPS and UMTS. It is well known that the stub-loaded resonator is used to generate multiple modes microstrip resonators BPF [3]. This behavior of microstrip BPF will be used to carry out a new transformation of dual-band to tri-band BPF. Figure 8 shows the schematic view of the new compact tri-band BPF. The proposed BPF has two open stubs loaded resonators which are used to generate the 3rd band in the current filter with the same size. It uses a suitable embedded open stub with two resonator sections in the spiral-shaped resonator, and each one is a quad wavelength

at 2.1 GHz. The length and width of the open stub line are $L_{S7} = 5.5$ mm and $W_{S7} = 0.8$ mm as in Figure 8, which lead to a compact structure as well as reduced insertion loss. The stub length L_{S7} of the microstrip stub-loaded resonator is used to tune the 3rd band which extends from 2.1 up to 2.45 GHz as in Figures 9(a), (b), because the 3rd resonance occurs when $L_{S7} \approx \lambda_{g3}/4$, where the λ_{g3} is the guided wavelength at the third resonant frequency which is given by:

$$f_{S3} = \frac{C}{\lambda_{g3}\sqrt{\varepsilon_{eff}}} \approx \frac{C}{4L_{S7}\sqrt{\varepsilon_{eff}}} \tag{5}$$

The upper two pass bands are electrically tuned by L_{M2}, while the performance of the fundamental lower passband remains constant at a center frequency of 0.75 GHz as in Figures 10(a), (b).

In addition, L_{S7} values have remarkable effect on the resulting filter performance. Figure 11(a) shows the resulting S_{11} and S_{21} responses corresponding to open circuit stub and listed in Table 1. It is obvious that its effect is much more noticeable on magnitudes of the transmission zeros, return loss and insertion loss. This parameter, L_{S7}, can be used to minimize insertion loss and maximize return loss. Furthermore, these resonators can offer multiple pass bands and transmission zeros and enhanced stopband attenuation up to 5 GHz. The simulated and measured results of the tri-band filter are plotted in Figure 11(a), and good agreement between them is observed. Figure 11(b) shows a photograph of the fabricated tri-band filter, with total size of $24.15 \times 12 \times 0.635\,\text{mm}^3$.

To understand which part of the filter is utilized at each operating frequency band, the surface current distributions are presented in Figure 12. These responses have been investigated using CST 2012, where red and blue colors indicate the highest and lowest effects, respectively. It is seen that the current distribution is concentrated consecutively on the spiral-shaped resonators at 0.75 GHz as in Figure 12(a), meander stub line at 1.21 GHz in Figure 12(b), and open circuit stub at 2.1 GHz

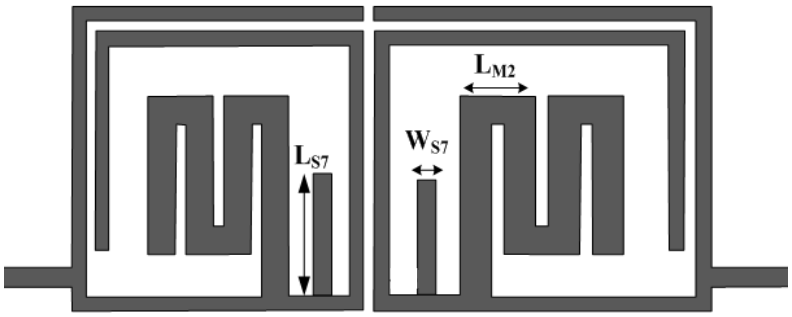

Figure 8. Topology of the proposed tri-band filter.

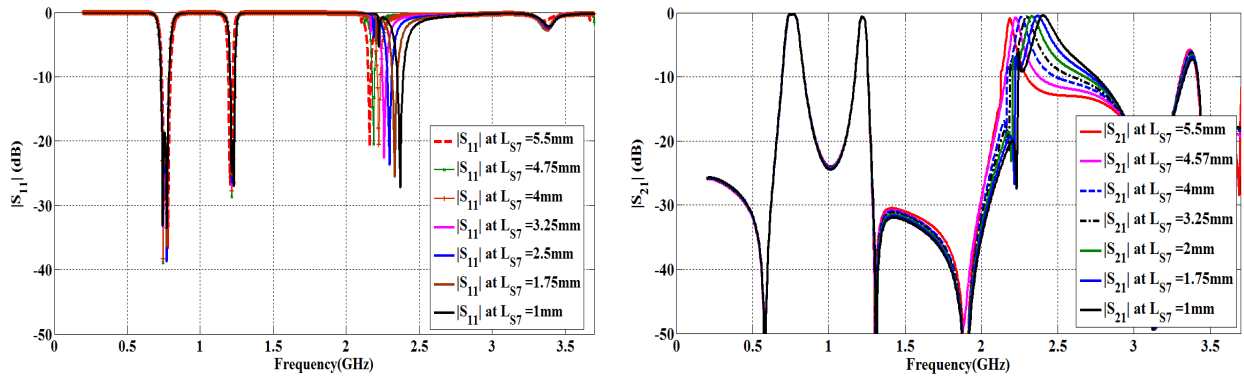

Figure 9. Different frequency responses with variation of open stub length L_{S7}, (a) S_{11}, (b) S_{21}.

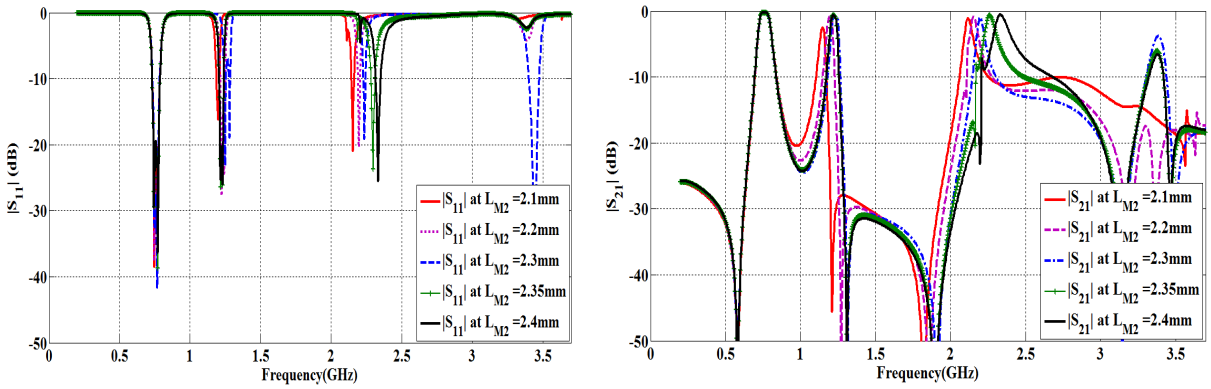

Figure 10. S-parameters of the tri-band for different meander stub length (L_{M2}), (a) S_{11}, (b) S_{21}.

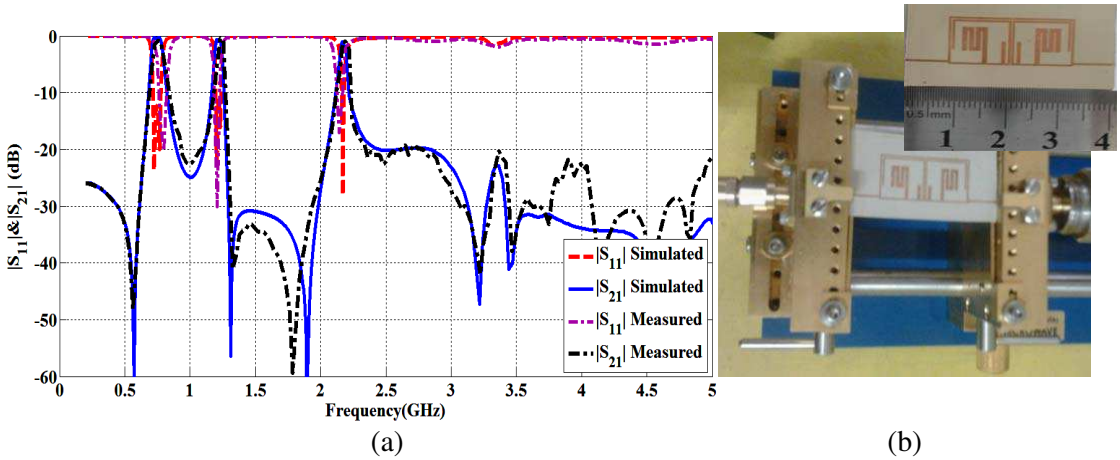

Figure 11. (a) Measured frequency response of the proposed tri-band BPF. (b) A photograph of the fabricated tri-band filter.

Table 1. Results of tri-band filters response.

Band	Band I	Band II	Band III
Resonant Frequency (GHz)	0.75	1.21	2.1
-3 dB band width (MHz)	96	45	54
Fractional BW (%)	12.5	4.5	2.6
Maximum Insertion loss (dB)	1	0.9	1.2
Transmission zero level (dB)	$-67/-23$	$-23/-46$	$-61/-42$

frequencies as in Figure 12(c). These three figures show that the positions of the first, the second and third resonant frequencies are controlled by adjusting the length of its corresponding line.

6. RESULTS AND DISCUSSION

A dual/tri band BPF using stub loaded resonator technique with spiral-shaped resonators and imbedded meander stub line matched to LTE 750 MHz, L_2 band GPS 1.21 GHz and UMTS 2.1 GHz commercial mobile satellite applications used in navigations and Mari time is designed. The bandpass filter is

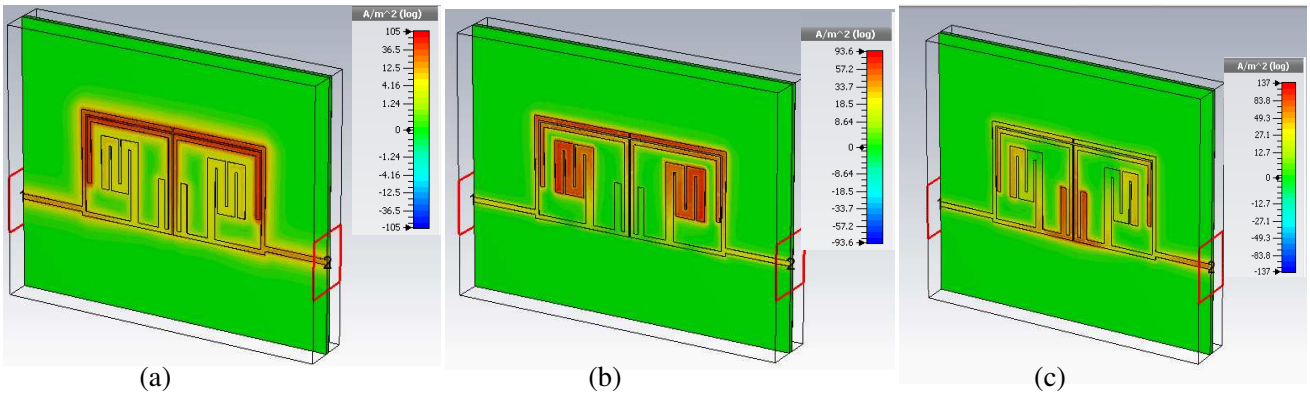

(a) (b) (c)

Figure 12. 3D surface current distribution of the tri-band BPF at different frequencies, (a) 0.75 GHz, (b) 1.21 GHz, and (c) 2.1 GHz.

Table 2. Dimensions of the tri-band filter after optimization (all dimensions in mm).

L_{S1}	L_{S2}	L_{S3}	L_{S4}	L_{S5}	d	t_1	t_2	t_2	W_S	W_M	L_{M1}	L_{M2}	L_{M3}
11.2	12	10.3	10.4	7	0.4	0.15	0.2	0.3	0.5	0.9	9	2.3	6
L_{M4}	W_{S5}	W_{S6}	L_{S6}	r	L_{S7}	W_{S7}							
4	2.2	0.8	3.35	0.25	5.58	0.83							

Table 3. Comparisons of the proposed filter with other reported tri-band filter.

	1st/2nd/3rd bands (GHz)	$\|S_{21}\|$ (dB)	$\|S_{21}\|$ (dB)	FBW (%)	T. Zero	Dimensions $(\text{mm})^2$
Ref. [7] 2007	1/2.5/3.6	2.2/1.8/1.7	20/40/35	5/2.1/1.4	2	60×60
Ref. [8] 2008	1/2.5/3.6	2.2/1.9/1.7	15/35/20	5/2.1/1.4	2	40×40
Ref. [9] 2009	2.4/4.8/7.2	1.7/0.9/0.7	15/23/18	5.3/6/8.7	5	22×15
Ref. [10] 2011	2.5/3.5/5.2	2/2.4/1.7	18/16/13	2.5/1.7/5	6	22×30
Ref. [11] 2012	2.5/3.5/5.9	2.1/1.9/2.3	18/30/22	3.5/3.8/4.5	9	60×60
Ref. [12] 2012	1.5/2.4/3.5	1.6/1.5/2.3	9/18/13.7	5.2/3.8/4.6	5	49.5×56.2
Ref. [13] 2012	1.8/2.7/3.5	2.2/2.1/1.3	14/13/9	3.9/2.9/4	7	37.5×27.8
Proposed filter	0.75/1.2/2.1	0.86/1/1.32	15/19/22	10/8/2.6	5	24.15×12

transformed from single/dual/tri bands with the same size. It is designed and fabricated on Rogers substrate (RO3010) with thickness of 0.635 mm, relative dielectric constant of 10.2, loss tangent = 0.0023 and 0.5 OZ of copper metallization thickness of 0.017 mm and simulated using CST 2012. The overall filter dimensions is 24.15 mm × 12 mm ($0.15\lambda_g \times 0.075\lambda_g$) with 64% reduction in size as compared to the same traditional size of 40.2 mm × 20 mm ($0.25\lambda_g \times 0.125\lambda_g$). After optimization, the dimensions of the proposed BPF with SLR implementation are listed in Table 2.

The measurements were done using the Agilent 7819ES Network Analyzer with frequency range 50 MHz to 13.5 GHz. The proposed filter shows at the frequencies, where transmission zeros exist, $S_{21} = 0$. To fulfill the condition, additional, transmission zeros near the two pass bands are generated by short stub loaded with via holes, due to the counteraction between electric and magnetic fields. These transmission zeros improve selectivity and cause suppression of the higher order modes. Table 3 summarizes comparisons of the proposed filter with other reported tri-band filters [7–12] and [13]. The proposed filter has the advantages of low insertion loss and compact size.

7. CONCLUSION

This paper presents a novel single-band to multi-band filter transformation method using stub loaded resonators. We can enhance the selectivity by generating two transmission zeros by adding two short circuit stubs with via holes. To demonstrate its potential, multi-band with high stopbands have been designed and fabricated. Three passbands with central frequencies of 0.75 GHz, 1.21 GHz and 2.1 GHz for commercial applications are achieved. The circuit structure exhibits good passband selectivity by the transmission zeros. The stopband characteristics of this filter are less than −20 dB up to 5 GHz in simulation results. The measurements show good consistency with the simulations. Therefore, it is expected that the proposed structure with its characteristics will be a strong candidate for applications in various integrated microwave circuits, with high-performance RF front-end, wide attenuation frequency bandwidth which make it suitable for modern RF and microwave satellite and mobile communication systems.

REFERENCES

1. Hasan, A. and A. E. Nadeem, "Novel microstrip hairpinline narrowband bandpass filter using via ground holes," *Progress In Electromagnetics Research*, Vol. 78, 393–419, 2008.
2. Zhang, X. Y., J. Shi, J.-X. Chen, and Q. Xue, "Dual-band bandpass filter design using a novel feed scheme," *IEEE Microw. Wireless Compon. Lett.*, Vol. 19, No. 6, 350–352, Jun. 2009.
3. Hong, J. S. and M. J. Lancaster, *Microstrip Filter for RF/Microwave Applications*, 2nd Edition, John Wiley & Sons, New York, 2011.
4. Girdhari, C. and J. Kim, "Design of dual-band bandpass filter using DGS with controllable second passband," *IEEE Microw. Wireless Compon. Lett.*, Vol. 21, No. 11, 589–591, Nov. 2011.
5. Dai, G. and M. Xia, "Novel miniaturized bandpass filters using spiral-shaped resonators and window feed structures," *Progress In Electromagnetics Research*, Vol. 100, 235–243, 2010.
6. Ma, D., Z. Y. Xiao, L. Xiang, X. Wu, C. Huang, and X. Kou, "Compact dual-band bandpass filter using folded SIR with two stubs for WLAN," *Progress In Electromagnetics Research*, Vol. 117, 357–364, 2011.
7. Lin, M. and Q. X. Chu, "Design of triple-band bandpass filter using tri-section stepped-impedance resonators," *Proc. Int. Microw. Millimeter Wave Tech. Conf.*, 798–800, Guilin, China, Apr. 2007.
8. Chu, Q. X. and X. M. Lin, "Advanced triple-band bandpass filter using tri-section SIR," *Electron. Lett.*, Vol. 44, No. 4, 295–296, Feb. 2008.
9. Chen, F. C. and Q. X. Chu, "Design of compact tri-band bandpass filters using assembled resonators," *IEEE Microw. Theory Tech.*, Vol. 57, No. 1, 165–171, Jan. 2009.
10. Luo, S., L. Zhu, and S. Sun, "Compact dual-mode triple-band bandpass filters using three pairs of degenerate modes in a ring resonator," *IEEE Trans. Microw. Theory Tech.*, Vol. 59, No. 5, 1222–1229, May 2011.
11. Li, Z.-P., S.-J. Wang, T. Su, and C.-H. Liang, "A novel triple passband filter design method based on stepped impedance resonators," *Progress In Electromagnetics Research C*, Vol. 33, 199–211, 2012.
12. Yu, W., M.-H. Weng, and S.-J. Chang, "A new tri-band bandpass filter based on stub-loaded step-impedance resonator," *IEEE Microw. Wireless Compon. Lett.*, Vol. 22, No. 4, 179–181, Apr. 2012.
13. Chen, W.-Y., M.-H. Weng, S.-J. Chang, H. Kuan, and Y.-H. Su, "A new tri-band bandpass filter for GSM, WIMAX and ultra-wideband responses by using asymmetric stepped impedance resonators," *Progress In Electromagnetics Research*, Vol. 124, 365–381, 2012.
14. Tsai, C.-M., S.-Y. Lee, and C.-C. Tsai, "Performance of a planar filter using a zero-degree feed structure," *IEEE Trans. Microw. Theory Tech.*, Vol. 50, No. 10, 2362–2367, Oct. 2002.